

Out-of-Distribution Detection using Counterfactual Distance

Maria Stoica, Francesco Leofante, Alessio Lomuscio

Imperial College London
m.stoica22@imperial.ac.uk, f.leofante@imperial.ac.uk, a.lomuscio@imperial.ac.uk

Abstract

Accurate and explainable out-of-distribution (OOD) detection is required to use machine learning systems safely. Previous work has shown that feature distance to decision boundaries can be used to identify OOD data effectively. In this paper, we build on this intuition and propose a post-hoc OOD detection method that, given an input, calculates the distance to decision boundaries by leveraging counterfactual explanations. Since computing explanations can be expensive for large architectures, we also propose strategies to improve scalability by computing counterfactuals directly in embedding space. Crucially, as the method employs counterfactual explanations, we can seamlessly use them to help interpret the results of our detector. We show that our method is in line with the state of the art on CIFAR-10, achieving 93.50% AUROC and 25.80% FPR95. Our method outperforms these methods on CIFAR-100 with 97.05% AUROC and 13.79% FPR95 and on ImageNet-200 with 92.55% AUROC and 33.55% FPR95 across four OOD datasets.

Introduction

As deep neural networks (DNNs) are more widely used in critical applications, research domains in DNN safety have emerged to combat unsafe outcomes and create reliable AI systems. Methods in DNN verification aim to make safety assurances at design time (Liu et al. 2021). These typically assume no distribution shift in the operating condition of the model. Handling distribution shift safely and reliably is, however, a big concern for runtime operations. The research areas of out-of-distribution (OOD) detection and monitoring are interested in developing methods and tools to tackle this issue. Specifically, OOD detection aims to find data points that differ from the in-distribution (ID) data that the DNN has been trained on (Amodei et al. 2016; Hendrycks and Gimpel 2017).

Several OOD detection methods exist. Their common aim is to differentiate between ID and OOD data using different techniques. One such category of detectors is *post-hoc* detectors, which are able to be used on pre-trained models due to the fact that they are not involved in the training process. We focus on these types of detectors in this work. These detectors use various methods; we present a small overview of some techniques in the related works section below, but refer to (Yang et al. 2024) for a more comprehensive discussion.

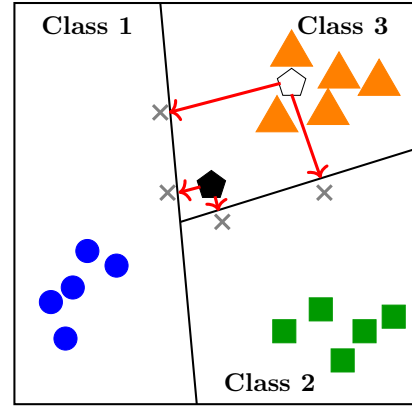


Figure 1: We present an instantiation of our framework with a toy example of a three class classification problem. In-distribution points are represented by the coloured circles, triangles, and squares. We then consider two new inputs: one OOD input (black pentagon) and one ID (white pentagon). Assume both inputs are initially classified as class 3. In this example we compute two counterfactuals (the grey crosses) for each input, one for class 1 and one for class 2, and compute the distances to these counterfactuals. We observe that the OOD input is closer to the decision boundaries and thus results in a smaller average counterfactual distance. Instead, the ID input is further away from the decision boundaries and thus, will have a greater average counterfactual distance than the anomaly point. In this paper, we leverage this intuition to build an OOD detection method that uses counterfactual distances as OOD scores to identify anomalies.

While the current state-of-the-art in OOD detection achieves good performance on a variety of measures, many crucially fall short in providing an explanation as to why a particular input is rejected. This hinders the ability to act on some detections in all scenarios where humans are in the loop to control the system (Ruff et al. 2021). To alleviate this issue, we propose an OOD detector that utilises methods from the explainability domain in order to not only detect OOD points, but also explain why they were flagged as OOD. Our OOD detector uses counterfactual distance (the distance between an input and its counterfactuals) as

an OOD score, simulating the distance from a point to decision boundaries. Several works have shown a correlation between a point being OOD and being further from ID points and closer to decision boundaries (Sun et al. 2022; Liu and Qin 2024). As we report in this paper, the counterfactual distance is more accurate than the approximated distances used by other methods, e.g., (Liu and Qin 2024), and leads to better ID versus OOD separability. Crucially, we can use the counterfactuals generated by our method to explain why the input was flagged as OOD without incurring any additional cost. We present an illustration of our approach in Figure 1 to help visualise our method.

There have been some works in tackling the explainability of OOD detectors, by outputting heatmaps (Liznerski et al. 2021) or generating counterfactual explanations after a point has been classified as OOD (Liznerski et al. 2024). However, by using counterfactual explanations to compute OOD detection scores, our method can both detect OOD points and explain them through counterfactuals without added overhead.

Contributions. In summary, our contribution is as follows:

- We present a post-hoc counterfactual-distance based OOD detection method, including both a method to compute these distances in input space and a method to reduce runtime costs by computing them in the embedding space.
- We show that we outperform state-of-the-art methods on a variety of widely used benchmarks, including CIFAR-10 and CIFAR-100 (Krizhevsky and Hinton 2009), and ImageNet-200 (Zhang et al. 2024), a subset of ImageNet-1K (Deng et al. 2009).
- We propose an explanation framework for our OOD detector. We illustrate how, by using the counterfactuals generated as part of the detection process, we can enhance the interpretability of the OOD detection without added runtime costs, thereby leading to more directly interpretable results.

The rest of the paper is organised as follows. Below, we introduce a brief discussion on related works. We then introduce the necessary background on DNNs, OOD detection, and counterfactual explanations in section . In section we present our method and explain how we utilise counterfactual distance to generate an OOD score. Then, in section , we evaluate our method against commonly used baselines and datasets. We also present our explanation framework along with a case study.

Related Work. A primary approach in OOD detection involves defining a score function based on the outputs of a Deep Neural Network. For example, the Maximum Softmax Probability (MSP) (Hendrycks and Gimpel 2017) uses a simple threshold on the highest softmax score, while ODIN (Liang, Li, and Srikant 2018) enhances this by applying temperature scaling and input perturbations to increase the separation between in-distribution and OOD data. Energy-based scoring offers another popular alternative (Lee et al. 2018). A key limitation of these methods, however, is

their vulnerability to model overconfidence, where a model can produce erroneously high-confidence predictions for OOD inputs (Nguyen, Yosinski, and Clune 2015).

To address this and produce more robust scores, a second line of work focuses on reducing noise by pruning or re-weighting neuron activations. ReAct (Sun, Guo, and Li 2021) clips high-magnitude activations in the penultimate layer, observing that OOD inputs tend to produce activations with higher variance than their in-distribution counterparts. Going further, other methods assess the importance of different network components. DICE (Sun and Li 2022) prunes noisy activations by ranking weights based on their contribution, while LiNe (Ahn, Park, and Kim 2023) employs Shapley values to identify the most salient neurons before applying activation clipping.

Distance-based methods have also emerged as a top-performing method. These approaches score inputs based on their distance to the training data’s distribution in some feature space. This includes using the k -th nearest neighbour distance in the model’s embedding space as an OOD score (Sun et al. 2022). The Fast Decision Boundary based Detector (fDBD) (Liu and Qin 2024) calculates an approximate distance to class decision boundaries, leveraging the insight that OOD points often reside closer to these boundaries than in-distribution points. Our work advances this concept by computing a more precise counterfactual distance to the decision boundary, which in turn yields a more discriminative OOD score.

The use of counterfactuals for the OOD detection task itself is a key novelty of our work. While counterfactual distance has been explored in adjacent domains, such as for membership inference attacks (Pawelczyk, Lakkaraju, and Neel 2023), its role in OOD has been confined to post-hoc explanation. For instance, recent frameworks propose generating counterfactuals to interpret and explain *why* a pre-existing detector flagged an input as an anomaly (Liznerski et al. 2024). While this aids interpretability, it does not contribute to the detection process itself. In contrast, our method is the first to integrate the counterfactual distance directly into the core scoring function. This holistic approach allows us to produce both a state-of-the-art OOD score and an explanation simultaneously, without incurring additional runtime costs.

Background

In this section, we define the notation to be used throughout this work and cover the necessary background for this paper. We introduce DNN notation and then illustrate OOD detection. Finally, we introduce counterfactual explanations.

Neural Networks. We consider a d -dimensional input space $\mathcal{X} \subseteq \mathbb{R}^d$ and output space $\mathcal{Y} = \{1, 2, \dots, C\}$ of classes (Goodfellow, Bengio, and Courville 2016). Let \mathcal{D}_{train} be a set of m labelled training samples $\{(x^{(1)}, y^{(1)}), \dots, (x^{(m)}, y^{(m)})\}$ where each $x^{(i)} \in \mathcal{X}$ and each $y^{(i)} \in \mathcal{Y}$. Furthermore, let $f : \mathcal{X} \rightarrow \mathcal{Y}$ be a DNN trained on \mathcal{D}_{train} and $f_{-1}(x)$ be the function returning the output of the penultimate layer of a DNN.

OOD Detection. Once a DNN is deployed and used in the real world, it may encounter inputs unlike those it was trained and tested on. These types of inputs are considered OOD. The goal of DNN OOD detection is to identify the outputs for these points as unsafe predictions, which may result in a warning system or require human intervention. This is done by creating a score function $S : \mathcal{X} \rightarrow \mathbb{R}$ whose output is used to determine whether an input is OOD or not:

$$\forall x \in \mathcal{X}, d(x) = \begin{cases} \text{ID} & \text{if } S(x) \geq \tau \\ \text{OOD} & \text{otherwise} \end{cases} \quad (1)$$

where $d(x)$ is an OOD classifier and τ is a threshold.

Counterfactual Explanations. A counterfactual explanation shows how the input of a DNN can be minimally changed in order to alter its output (Wachter, Mittelstadt, and Russell 2017).

Definition 1 (Counterfactuals). *Given an input $x \in \mathcal{X}$, a trained DNN f , and a distance function $\text{dist} : \mathbb{R}^n \times \mathbb{R}^n \rightarrow \mathbb{R}^+$, $x' \in \mathcal{X}$ is a counterfactual for x such that*

$$\arg \min_{x'} \text{dist}(x, x') \text{ subject to } f(x) \neq f(x'). \quad (2)$$

Usually, the counterfactual is chosen such that x' is also close to x by some distance metric such as Manhattan or Euclidean distance (see, e.g., (Guidotti 2024) for a recent survey). Many methods of counterfactual search exist, and we will discuss some of these in section and evaluate them within our framework in section .

OOD Detection using Counterfactual Distance

In this section, we introduce our post-hoc counterfactual distance measure. We first show how to calculate our score in input space and then introduce a variant where we calculate the distance in embedding space to reduce runtime costs.

Measures of distance have been used in the literature to inform whether an input is OOD or not. In particular, some methods look at the distance between an input and the decision boundaries, postulating that DNNs are uncertain about points that reside close to these boundaries (Liu and Qin 2024). While previous methods use approximations to calculate distances, we propose a more accurate distance measure to the decision boundary. Specifically, we calculate the distance of an input to the decision boundary by finding a counterfactual for the point to a given target output. Our method reinforces the notion that ID features tend to be further away from the decision boundary than OOD features. This method is post-hoc, meaning it is independent of the training procedure and can readily be used on any pre-trained DNN, regardless of its architecture. Our method is based on the theoretical framework established by (Liu and Qin 2024). For a comprehensive discussion of the underlying principles, we refer the reader to their original work.

Counterfactual Distance Measure

Naturally, the first inclination is to compute counterfactual distances directly on the input space. For an input x , we do this by taking the output of the pre-trained DNN, $f(x)$, and

generate counterfactuals for each class in \mathcal{Y} that is not equal to the output of the network on the input, $f(x)$. The distances are computed using the l_2 norm and then we take the average and also regularise the scores following the methodology of (Liu and Qin 2024). This regularisation is done by computing μ_{train} , the mean of the input features of the training dataset, and computing the distance between x and μ_{train} . Thus, our counterfactual distance measure is calculated as:

$$\frac{1}{|\mathcal{Y}| - 1} \sum_{y \in \mathcal{Y}, y \neq f(x)} \frac{\|CF(x, y) - x\|_2}{\|x - \mu_{train}\|_2} \quad (3)$$

where $CF(x, y)$ is a function returning a counterfactual on an input x for a target class y .

However, computing counterfactuals in the input space may be costly depending, e.g., on the number of input features and the size of the DNN. We discuss how the runtime of the counterfactual search method is impacted by these parameters at the end of this section. To reduce the runtime of our method, we also propose an alternative distance measure by moving to the embedding space.

Moving to Embedding Space. While we started our analysis on input space, we moved to embedding space to reduce the dimensionality of our calculations. For each input x , we compute counterfactuals on $f_{-1}(x)$, the output of the penultimate layer of the DNN, instead of directly on x , which gives us a counterfactual in the embedding space. In equation 4, we show how we take these counterfactual distances, similarly to what we did in input space.

$$\frac{1}{|\mathcal{Y}| - 1} \sum_{y \in \mathcal{Y}, y \neq f(x)} \frac{\|CF(f_{-1}(x), y) - f_{-1}(x)\|_2}{\|f_{-1}(x) - \mu_{train}\|_2} \quad (4)$$

where $CF(f_{-1}(x), y)$ is a function returning a counterfactual on $f_{-1}(x)$ with target class y . When we move to the embedding space, μ_{train} is the mean over the training set in the embedding space, rather than in the input space.

We present the procedure for calculating the embedding-space OOD score in Algorithm 1. The function `GetCounterfactual` takes in the embedding z_x and a target class, y , from the known classes of the DNN excluding the predicted class for the input x . We then use `GetDistance` to get the l_2 distance between z_x and its counterfactual and take the average over the number of counterfactual distances we compute. After we compute this distance, we normalise it with respect to the distance from the input to the mean of the training set in embedding space, which is precomputed.

On top of the reduction in runtime, we found that by taking counterfactual distance from a close to output layer of the DNN, we were able to better separate the ID and OOD data. This finding is in line with other methods that use close-to-output-layer activations to improve OOD separability (Henzinger, Lukina, and Schilling 2020; Liu and Qin 2024). Moving our counterfactual distance calculation to the embedding space creates a more accurate and efficient method than computing distances on the input space.

Remark. The runtime of our approach is dependent on our choice of counterfactual explanation method,

Algorithm 1: Counterfactual distance measure

Input: Sample input x
Known classes $\mathcal{Y} = \{1, 2, \dots, C\}$
Pre-trained DNN f
Output: OOD score D

```
1:  $z_x \leftarrow f_{-1}(x)$ 
2:  $D \leftarrow 0$ 
3: for  $y \in \{\mathcal{Y} \setminus f(x)\}$  do
4:    $c_{x,y} \leftarrow \text{GetCounterfactual}(z_x, y)$ 
5:    $D \leftarrow D + \text{GetDistance}(z_x, c_{x,y})$ 
6: end for
7: return  $D$ 
```

whether it is based on Mixed Integer Linear Programming (MILP) (Mohammadi et al. 2021), gradient-based optimisations (Wachter, Mittelstadt, and Russell 2017), or nearest neighbors (Brugmans, Leyman, and Martens 2024). For example, approaches that use MILP are NP-complete whereas nearest-neighbour based counterfactual search methods have a runtime that is quadratic in the number of features of the input (Leofante and Potyka 2024). The choice of counterfactual method is crucial to the efficiency of calculating our OOD score, as it dominates the runtime, both in input space and in embedding space. In section , we will show how the choice of counterfactual method impacts the accuracy and runtime of our OOD detector.

Evaluation

In the previous section, we described how to compute a counterfactual-distance-based OOD score and methods by which to reduce the runtime costs of our scoring system. In this section, we evaluate our method using the embedding space calculations against several standard baselines on commonly used datasets for OOD detection.

We evaluate our method in the following experiments:

- In section experiments were run with our embedding-space OOD score on both CIFAR-10 and CIFAR-100 (Krizhevsky and Hinton 2009). We demonstrate the accuracy of our method against the state-of-the-art.
- In section we present results on the ImageNet-200 benchmark comparing against eight baseline methods and commonly used OOD datasets.
- Finally, in section , we show how our counterfactuals can be used to generate explanations. We present an example of an explanation our method can produce with MNIST.

Experimental Setup

Datasets and Architectures. To ensure a rigorous and direct comparison against the state of the art, our experimental protocol is aligned with the standards established by leading contemporary works in this area (Zhang et al. 2024). We evaluate our method on CIFAR-10, CIFAR-100 (Krizhevsky and Hinton 2009), and ImageNet-200 (Zhang et al. 2024), using pre-trained ResNet-18 models (He et al. 2016) provided by OpenOOD (Yang et al. 2022). For each benchmark, we use four standard OOD datasets for evaluation.

We also use MNIST (LeCun, Cortes, and Burges 1998) for a case study with a custom 3-layer CNN. Full details on the datasets and DNNs can be found in the appendix.

Counterfactual and Baseline Methods. Our detector is evaluated using two nearest-neighbour-based counterfactual explanation methods: NICE (Brugmans, Leyman, and Martens 2024) and NNCE (Guidotti 2024). We focus on nearest neighbour methods due to their lower runtime costs compared to other methods such as MILP-based. However, our detector can be easily extended to use any counterfactual explanation method. Implementation details of these methods are included in the appendix. We compare our method against eight state-of-the-art baselines, including MSP (Hendrycks and Gimpel 2017), ODIN (Liang, Li, and Srikant 2018), Energy (Liu et al. 2020), and fDBD (Liu and Qin 2024). A complete list and description of baseline methods can be found in the appendix. All experiments were conducted on a machine with an AMD EPYC 7453 28-Core CPU and 512GB of RAM.

Evaluation on CIFAR Benchmarks

In this section, we provide experimental results on the accuracy of our method versus some commonly utilised benchmarks on both CIFAR-10 and CIFAR-100. For both datasets, we average over three pre-trained ResNet-18 (He et al. 2016) networks provided by OpenOOD (Yang et al. 2022). We also utilise OpenOOD’s API to obtain our results for the eight state-of-the-art methods we compare against for consistency.

CIFAR-10 Results. For our evaluation on CIFAR-10, we use the test set of 10,000 images for our ID samples. Results can be found in Table 1, where we report results on the four OOD datasets and averages. Our method outperforms all baselines against SVHN and iSUN and, on average, is in line with the results of fDBD, KNN, and ViM.

The results are generally stronger when comparing our method to the methods that score model uncertainty (MSP, ODIN, and Energy). The FPR95 and AUROC for our method show more accuracy on the Textures dataset than ODIN and Energy and marginally outperform MSP. On the Places365 dataset, MSP outperforms with a 42.46% FPR95 versus our NICE method with 48.57% FPR95. However, on average, our method outperforms these methods.

Overall, on Places365 and Textures, we see that ViM, MDS, KNN, and fDBD outperform our method. On Textures, our reported FPR95 is 34.98% versus 21.14% with ViM and on the Places365 dataset, our method produces a 48.57% FPR95 while fDBD achieves 29.16%. On average, we are competitive across all methods, with fDBD, KNN, and ViM outperforming our method by about 1.99%, 1.73%, and 0.12%, respectively.

Comparing NICE and NNCE, we see that NICE gave us slightly better results overall, but the NNCE method is comparable. The most significant difference between the two is on the Places365 dataset, where we see a 12.02% difference in FPR95. While the results on CIFAR-10 are not consistently outperforming other methods, the results are best on SVHN using NICE with 5.69% FPR95 and on iSUN using NNCE with 13.69% FPR95, respectively. To illustrate these

Method	SVHN		iSUN		Textures		Places365		Average	
	FPR95↓	AUROC↑	FPR95↓	AUROC↑	FPR95↓	AUROC↑	FPR95↓	AUROC↑	FPR95↓	AUROC↑
MSP	25.43	91.56	23.05	92.36	35.22	89.89	42.46	88.92	31.54	90.68
ODIN	68.54	84.70	27.20	94.63	67.89	86.94	70.40	85.08	58.51	87.84
Energy	34.20	91.98	27.69	93.24	52.01	89.46	54.69	89.25	42.15	90.98
ViM	19.01	94.58	21.12	94.20	21.14	95.16	41.44	89.50	25.68	93.36
MDS	25.88	91.17	32.09	90.11	28.03	92.69	47.69	84.91	33.42	89.72
KNN	22.39	92.77	19.48	94.57	24.06	93.16	30.35	91.77	24.07	89.24
DICE	36.16	90.22	59.60	81.26	62.73	81.88	77.21	74.74	58.93	82.02
fDBD	22.50	92.93	19.24	94.57	24.35	93.13	29.16	92.01	23.81	93.16
Ours + NICE	5.69	98.66	13.96	97.18	34.98	91.34	48.57	86.79	25.80	93.50
Ours + NNCE	5.79	98.55	13.69	97.01	37.83	88.99	60.59	80.49	29.47	91.26

Table 1: Evaluation on CIFAR-10. We use the OpenOOD implementation for all benchmarks and average the values over three training runs from their saved models. We give results on our method using two different counterfactual search methods, NICE and NNCE. The best results are in bold.

Method	SVHN		iSUN		Textures		Places365		Average	
	FPR95↓	AUROC↑	FPR95↓	AUROC↑	FPR95↓	AUROC↑	FPR95↓	AUROC↑	FPR95↓	AUROC↑
MSP	58.43	78.68	51.05	82.06	61.79	77.32	56.65	79.21	56.98	79.32
ODIN	67.18	74.72	35.50	90.65	62.41	79.34	59.73	79.45	56.21	81.04
Energy	53.19	82.28	45.53	85.82	62.39	78.35	57.69	79.50	54.70	81.49
ViM	46.37	82.87	46.64	82.13	47.22	85.75	61.57	75.86	50.45	81.65
MDS	67.47	70.32	77.48	63.77	70.21	76.42	79.19	63.41	73.59	68.48
KNN	51.48	84.26	47.47	84.26	53.63	83.66	60.76	79.42	53.33	82.90
DICE	48.96	84.45	46.13	85.37	64.26	77.63	59.42	78.31	54.69	81.44
fDBD	53.53	80.67	41.36	86.10	53.60	81.18	57.18	79.85	51.42	81.95
Ours + NICE	0.40	99.86	3.40	99.31	34.67	93.17	50.75	88.78	22.30	95.28
Ours + NNCE	0.04	99.99	0.44	99.80	19.21	95.88	35.47	92.54	13.79	97.05

Table 2: Evaluation on CIFAR-100. We use the OpenOOD implementation for all benchmarks and average the values over three training runs from their saved models. We give results on our method using two counterfactual search methods, NICE and NNCE. The best results are in bold.

differences, we look at the OOD scores produced by both methods to compare the differences in calculated distances. The average OOD score using NICE on the ID data is 0.14, and on SVHN, it is 0.07. For NNCE, these numbers are 0.32 for ID data and 0.19. We see that NICE can find closer counterfactuals, as the distances are smaller than NNCE found.

CIFAR-100 Results. Our evaluation on CIFAR-100 shows promising results, increasing accuracy over all benchmarks on all OOD datasets. Our performance on CIFAR-100 stays consistent with our results from CIFAR-10, while other methods show a deterioration in accuracy.

In the previous set of experiments on CIFAR-10, we saw that ViM, KNN, MDS, and fDBD outperformed our method on some datasets. However, when evaluating our method on CIFAR-100, the results for both NICE and NNCE improve upon FPR95 and AUROC against all baseline methods. We hypothesize that this could be because computing distances to more decision boundaries can give more accuracy to our OOD score. On SVHN, we see the best results with NNCE achieving a 0.04% FPR95 and 99.99% AUROC, where the next best result, with ViM, shows a 19.01% FPR95 and a 94.58% AUROC. SVHN was similarly our best dataset on CIFAR-10.

Overall, looking at the average performance, our method achieves a 13.79% FPR95 and 97.05% AUROC, which is an improvement of 36.66% FPR95 compared to the next best method, ViM which achieves an FPR95 of 50.45%. This is approximately a 72.67% reduction in FPR.

The results on CIFAR-100 show the impact that a more accurate distance measure can have on the accuracy of the OOD score. Compared to fDBD, we show an improvement of 37.63% on FPR95 and 15.10% on AUROC.

While NICE outperformed NNCE on the CIFAR-10 experiments, we see that NNCE shows stronger results on CIFAR-100. We hypothesize that this outperformance is due to the structure of the underlying dataset, and these results show how accuracy is dependent on the choice of counterfactual search method. In section , we provide experiments on ImageNet-200 to see how our method performs on a larger dataset. We also include an ablation study on CIFAR-100 in the appendix to further investigate how we can reduce runtime costs.

Evaluation on ImageNet-200

In this section, we provide experimental results on ImageNet-200 with some commonly used OOD datasets

Method	SSB-hard		iNaturalist		Textures		OpenImage-O		Average	
	FPR95↓	AUROC↑	FPR95↓	AUROC↑	FPR95↓	AUROC↑	FPR95↓	AUROC↑	FPR95↓	AUROC↑
MSP	66.09	80.32	35.39	90.13	44.43	88.37	35.21	89.24	45.28	87.01
ODIN	73.52	77.17	22.49	94.34	42.96	90.67	37.29	90.10	44.07	88.07
Energy	69.97	79.72	26.41	92.52	41.29	90.80	36.80	89.20	43.62	88.06
ViM	71.59	74.00	26.81	91.38	20.19	94.77	33.96	88.21	38.14	87.09
MDS	83.60	58.52	58.13	75.34	58.13	79.25	67.87	70.15	66.93	70.81
KNN	73.90	76.88	24.43	93.97	24.52	95.30	32.94	90.17	38.95	89.08
DICE	71.02	78.95	29.74	91.77	40.79	91.54	38.82	89.03	45.09	87.82
fDBD	66.66	80.49	16.55	95.66	29.61	92.95	27.20	91.73	35.01	90.21
Ours + NNCE	73.61	80.60	23.55	96.32	35.48	93.65	1.55	99.63	33.55	92.55

Table 3: Evaluation on ImageNet-200. We use the OpenOOD implementation for all benchmarks and average the values over three training runs from their saved models. We give results on our method using the counterfactual search method NNCE. The best results are in bold.

in order to evaluate our method on a larger dataset. For this benchmark, we utilise a pre-trained ResNet-18 network from OpenOOD (Yang et al. 2022). We compare to the same eight baseline OOD detectors as we did in the previous section, also using the OpenOOD implementations of these methods. Due to runtime constraints introduced by utilising a larger dataset, we only provide results using the counterfactual search method NNCE.

We present our results on the four OOD datasets and the average results in Table 3. Our results show that our method outperforms the baselines on OpenImage-O with a 1.55% FPR95 and 99.63% AUROC, which is an improvement over the next best results with fDBD which obtained a 27.20% FPR95 and a 91.73% AUROC. We also obtain the best AUROC on SSB-hard with 80.60%, though our FPR95 is a bit higher than all methods except MDS and KNN. Similarly, our method has the highest AUROC on iNaturalist with 96.32%, though our FPR95 was a bit higher than ODIN and fDBD. On Textures, the best FPR95 is found with ViM with a 20.19% FPR95 and KNN has the best AUROC of 95.30%. Our results are comparable with a 35.48% FPR94 and 93.65% AUROC. fDBD also has a better FPR95 than ours, but a lower AUROC.

On average, we outperform the baselines over these four OOD datasets with an overall FPR95 of 33.55% and AUROC of 92.55%. These results show our method can separate ID and OOD data on larger and more complex datasets. Similarly to our experiments on the CIFAR benchmarks, these results also show that the structure of the underlying datasets cause some variance in performance. While some methods outperform ours on certain OOD datasets, our results are obtained via a counterfactual search method that finds an approximate counterfactual via nearest unlike neighbours, rather than a more optimised search. Thus, the distance we calculate to the decision boundary will be more coarse. The results could be further improved with a more exact counterfactual search, but this would increase runtime costs.

Generating Counterfactual Explanations

While our method shows promising results in accurately separating ID and OOD data, it also can serve as a tool

for interpreting results without added runtime costs. These counterfactuals we compute for our distance score can highlight what features of an OOD point are unlike the network’s known classes. This section presents a case study on generating explanations through our method on the MNIST dataset (LeCun, Cortes, and Burges 1998).

As our method computes counterfactuals in the embedding space, reporting these counterfactuals in the input space would require the training of an autoencoder, which would, in turn, increase the computational overhead of our method. Instead, we take advantage of NNCE and utilise the nearest unlike neighbours. We map the embedding representations of the training set back to their respective input representations at training time. Our explanation framework then works as follows: for an input flagged as OOD, we generate the k nearest unlike neighbours and the k nearest neighbours of the predicted class. This way, we can help an end user to see what the network is unsure about. By providing nearest unlike neighbours, we can answer the question *could this input have been anything else from the network’s knowledge?*

Case Study. We provide a case study on our framework using MNIST and describe how our explanation method can aid an end user. We set up these experiments by training a CNN on the first six classes (numbers 0-5), withholding classes 6-9 for OOD points. For our evaluation, we consider images in the test set belonging to the first six classes as ID points and the rest as OOD. We obtain an FPR95 of 44.26% and AUROC of 89.20% via this method.

Our explanation framework is as follows: for each point classed as OOD, we find the k nearest like neighbours and the k nearest unlike neighbours for the closest possible classes (or all possible classes if it is feasible). We present the OOD input with its neighbours, ranked by distance order, to help us understand why an input was classed as OOD. In the case of novelty detection, we can show that the input is unlike any of the neighbours, like or unlike. In the case of a distribution shift where the input’s ground truth is within the known classes of the DNN, we can show the closest classes to show why this input could have been misclassified and what about this OOD input is unusual. We present an example of novelty detection below; an example of a distribution

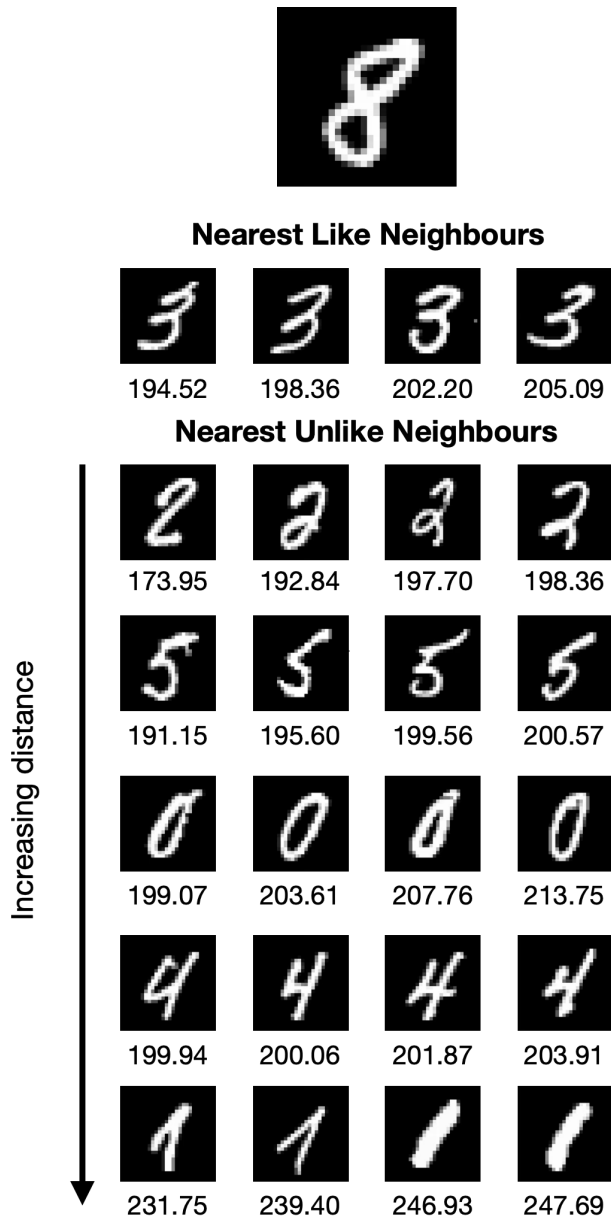


Figure 2: An example of an explanation our method can output. At the top, we have an OOD point, which is an 8 and a class our model is unaware of. The model predicts this to be a 3. Below the 8, we present the four nearest like neighbours, which are the closest 3s in the training set to our OOD input. The leftmost 3 is the closest to this 8, and the distance increases as we go to the right. Below this, we present each class’s four nearest unlike neighbours. The classes are ordered by how close they are to the original input, so the 2s are closest, followed by the 5s, and so on, with 1s being the furthest class. Within each class row, the leftmost image is the closest to the input, and the rightmost is the furthest. The input is closest to the 2s class, even compared to the 3s class. We present the distance between the nearest neighbour and the original input below each image. By utilising nearest like and unlike neighbours, we can reduce model over reliance and better understand why our detector identified this input as OOD.

shift is given in the appendix.

We present our framework on the following example from MNIST, where $k = 4$, meaning we obtain the four closest images for each class. This is illustrated in Figure 2. In this case, we have an image of an 8, which is novel to our DNN as it was not trained to recognise 8s. The DNN, in this case, labels this 8 as a 3. We gather four examples of the closest 3s (nearest like neighbours), ranked by distance, where the leftmost image is the closest to our input. Comparing the 8s to the 3s, we see some similarities, but it is quickly apparent that the 8 should not belong to this class. What about any other possible classes? We present the nearest unlike neighbours for each class known to our DNN. The nearest classes are in rows, ranked by distance where 2 is the closest unlike class to our input and 1 is the furthest. Within each row, the leftmost image is the closest. It is also interesting to note that in our example, the 2 class is closer to our input than the 3 class. This information can further reinforce that this 8 is indeed OOD to our model. By providing both factual and counterfactual images for our input, we can place more trust in the verdict that this input is OOD, as we can now see that this input is unlike any of the known classes.

Overall, our counterfactual-distance based scoring method is on par with or outperforms the state-of-the-art in OOD detection. It achieved promising results, specifically on CIFAR-100. However, our method stands out from the current baselines by providing interpretability as a by-product. We can produce counterfactual and factual explanations to aid end users in understanding why an input is OOD.

Discussion and Conclusion

In this paper, we introduced a novel method to perform OOD detection using counterfactual distance. We showed two variations of this method: one operating in input space and a more lightweight approach using the outputs of the penultimate layer of the network. Finally, we presented a framework to describe how we can easily generate explanations without added runtime costs to aid in determining why an input is classed as OOD. Our method outperforms the state-of-the-art on CIFAR and ImageNet-200 benchmarks, and we show methods to reduce the runtime costs of our method.

This paper opens interesting avenues for future work. One is investigating more lightweight counterfactual methods. Methods that can be optimised to run on GPUs for image-based counterfactual search would be important for runtime assurance and testing on larger datasets or more complex DNN architectures. It would also be important to investigate how utilising different methods of counterfactual search or how robust search methods would impact the accuracy of the OOD detector. We also believe it would be interesting to run a user study on our method to ascertain how valuable these explanations are and explore other ways to present our counterfactual explanations. This would help establish whether explanations help improve the interpretability of OOD detection.

Acknowledgments

This work was supported by the UK Research and Innovation [grant number EP/S023356/1] in the UKRI Centre for Doctoral Training in Safe and Trusted Artificial Intelligence (www.safeandtrustedai.org).

References

- Ahn, Y. H.; Park, G.-M.; and Kim, S. T. 2023. LINE: Out-of-Distribution Detection by Leveraging Important Neurons. In *2023 IEEE/CVF Conference on Computer Vision and Pattern Recognition (CVPR)*, 19852–19862. ISSN: 2575-7075.
- Amodei, D.; Olah, C.; Steinhardt, J.; Christiano, P.; Schulman, J.; and Mané, D. 2016. Concrete Problems in AI Safety.
- Brugmans, D.; Leyman, P.; and Martens, D. 2024. NICE: an algorithm for nearest instance counterfactual explanations. *Data Mining and Knowledge Discovery*, 38(5): 2665–2703.
- Cimpoi, M.; Maji, S.; Kokkinos, I.; Mohamed, S.; and Vedaldi, A. 2014. Describing Textures in the Wild. In *2014 IEEE Conference on Computer Vision and Pattern Recognition (CVPR14)*, 3606–3613.
- Deng, J.; Dong, W.; Socher, R.; Li, L.-J.; Li, K.; and Fei-Fei, L. 2009. ImageNet: A large-scale hierarchical image database. In *2009 IEEE Conference on Computer Vision and Pattern Recognition*, 248–255. ISSN: 1063-6919.
- Goodfellow, I.; Bengio, Y.; and Courville, A. 2016. *Deep Learning*. MIT Press.
- Guidotti, R. 2024. Counterfactual explanations and how to find them: literature review and benchmarking. *Data Mining and Knowledge Discovery*, 38(5): 2770–2824.
- He, K.; Zhang, X.; Ren, S.; and Sun, J. 2016. Deep Residual Learning for Image Recognition. In *2016 IEEE Conference on Computer Vision and Pattern Recognition (CVPR16)*. IEEE.
- Hendrycks, D.; and Gimpel, K. 2017. A baseline for detecting misclassified and out-of-distribution examples in neural networks. In *5th International Conference on Learning Representations (ICLR17)*.
- Henzinger, T. A.; Lukina, A.; and Schilling, C. 2020. Outside the Box: Abstraction-Based Monitoring of Neural Networks. In *24th European Conference on Artificial Intelligence (ECAI20)*.
- Krizhevsky, A.; and Hinton, G. 2009. Learning multiple layers of features from tiny images. *Technical Report, University of Toronto*.
- LeCun, Y.; Cortes, C.; and Burges, C. J. 1998. The MNIST database of handwritten digits.
- Lee, K.; Lee, K.; Lee, H.; and Shin, J. 2018. A Simple Unified Framework for Detecting Out-of-Distribution Samples and Adversarial Attacks. In *Advances in Neural Information Processing Systems (NeurIPS18)*.
- Leofante, F.; and Potyka, N. 2024. Promoting Counterfactual Robustness through Diversity. *Proceedings of the AAAI Conference on Artificial Intelligence (AAAI24)*.
- Liang, S.; Li, Y.; and Srikant, R. 2018. Enhancing the reliability of out-of-distribution image detection in neural networks. In *6th International Conference on Learning Representations (ICLR18)*.
- Liu, C.; Arnon, T.; Lazarus, C.; Strong, C.; Barrett, C.; and Kochenderfer, M. J. 2021. Algorithms for Verifying Deep Neural Networks. *Foundations and Trends in Optimization*.
- Liu, L.; and Qin, Y. 2024. Fast Decision Boundary based Out-of-Distribution Detector. In *Forty-first International Conference on Machine Learning (ICML24)*.
- Liu, W.; Wang, X.; Owens, J.; and Li, Y. 2020. Energy-based Out-of-distribution Detection. In *Advances in Neural Information Processing Systems (NeurIPS20)*.
- Liznerski, P.; Ruff, L.; Vandermeulen, R. A.; Franks, B. J.; Kloft, M.; and Muller, K. R. 2021. Explainable Deep One-Class Classification. In *International Conference on Learning Representations (ICLR21)*.
- Liznerski, P.; Varshneya, S.; Calikus, E.; Fellenz, S.; and Kloft, M. 2024. Reimagining Anomalies: What If Anomalies Were Normal?
- Mohammadi, K.; Karimi, A.-H.; Barthe, G.; and Valera, I. 2021. Scaling Guarantees for Nearest Counterfactual Explanations. In *Proceedings of the 2021 AAAI/ACM Conference on AI, Ethics, and Society (AIES21)*.
- Netzer, Y.; Wang, T.; Coates, A.; Bissacco, A.; Wu, B.; and Ng, A. Y. 2011. Reading Digits in Natural Images with Unsupervised Feature Learning. In *NIPS Workshop on Deep Learning and Unsupervised Feature Learning 2011*.
- Nguyen, A.; Yosinski, J.; and Clune, J. 2015. Deep Neural Networks are Easily Fooled: High Confidence Predictions for Unrecognizable Images. In *2015 IEEE Conference on Computer Vision and Pattern Recognition (CVPR15)*, 427–436. Boston, MA, USA: IEEE. ISBN 978-1-4673-6964-0.
- Pawelczyk, M.; Lakkaraju, H.; and Neel, S. 2023. On the Privacy Risks of Algorithmic Recourse. In *Proceedings of The 26th International Conference on Artificial Intelligence and Statistics (AISTATS23)*, 9680–9696. PMLR. ISSN: 2640-3498.
- Ruff, L.; Kauffmann, J. R.; Vandermeulen, R. A.; Montavon, G.; Samek, W.; Kloft, M.; Dietterich, T. G.; and Müller, K.-R. 2021. A Unifying Review of Deep and Shallow Anomaly Detection. *Proceedings of the IEEE*, 109(5): 756–795. Conference Name: Proceedings of the IEEE.
- Sun, Y.; Guo, C.; and Li, Y. 2021. ReAct: Out-of-distribution Detection With Rectified Activations. In *Advances in Neural Information Processing Systems (NeurIPS21)*, volume 34, 144–157. Curran Associates, Inc.
- Sun, Y.; and Li, Y. 2022. DICE: Leveraging Sparsification for Out-of-Distribution Detection. In Avidan, S.; Brostow, G.; Cissé, M.; Farinella, G. M.; and Hassner, T., eds., *Computer Vision – ECCV 2022*, Lecture Notes in Computer Science, 691–708. Cham: Springer Nature Switzerland. ISBN 978-3-031-20053-3.
- Sun, Y.; Ming, Y.; Zhu, X.; and Li, Y. 2022. Out-of-Distribution Detection with Deep Nearest Neighbors. In

Proceedings of the 39th International Conference on Machine Learning (ICML22), 20827–20840. PMLR. ISSN: 2640-3498.

Van Horn, G.; Mac Aodha, O.; Song, Y.; Cui, Y.; Sun, C.; Shepard, A.; Adam, H.; Perona, P.; and Belongie, S. 2018. The INaturalist Species Classification and Detection Dataset. 8769–8778.

Vaze, S.; Han, K.; Vedaldi, A.; and Zisserman, A. 2022. Open-Set Recognition: A Good Closed-Set Classifier is All You Need. In *International Conference on Learning Representations (ICLR22)*.

Wachter, S.; Mittelstadt, B.; and Russell, C. 2017. Counterfactual Explanations without Opening the Black Box: Automated Decisions and the GDPR. *Harvard Journal of Law & Technology (Harvard JOLT)*, 31(2): 841–888.

Wang, H.; Li, Z.; Feng, L.; and Zhang, W. 2022. ViM: Out-Of-Distribution with Virtual-logit Matching. In *2022 IEEE/CVF Conference on Computer Vision and Pattern Recognition (CVPR22)*, 4911–4920. New Orleans, LA, USA: IEEE. ISBN 978-1-66546-946-3.

Xu, P.; Ehinger, K. A.; Zhang, Y.; Finkelstein, A.; Kulkarini, S. R.; and Xiao, J. 2015. TurkerGaze: Crowdsourcing Saliency with Webcam based Eye Tracking. ArXiv:1504.06755 [cs].

Yang, J.; Wang, P.; Zou, D.; Zhou, Z.; Ding, K.; Peng, W.; Wang, H.; Chen, G.; Li, B.; Sun, Y.; Du, X.; Zhou, K.; Zhang, W.; Hendrycks, D.; Li, Y.; and Liu, Z. 2022. OpenOOD: Benchmarking Generalized Out-of-Distribution Detection. *Advances in Neural Information Processing Systems (NeurIPS22)*, 35: 32598–32611.

Yang, J.; Zhou, K.; Li, Y.; and Liu, Z. 2024. Generalized Out-of-Distribution Detection: A Survey. *International Journal of Computer Vision*, 132(12): 5635–5662.

Zhang, J.; Yang, J.; Wang, P.; Wang, H.; Lin, Y.; Zhang, H.; Sun, Y.; Du, X.; Li, Y.; Liu, Z.; Chen, Y.; and Li, H. 2024. OpenOOD v1.5: Enhanced Benchmark for Out-of-Distribution Detection. ArXiv:2306.09301 [cs].

Zhou, B.; Lapedriza, A.; Khosla, A.; Oliva, A.; and Torralba, A. 2018. Places: A 10 Million Image Database for Scene Recognition. *IEEE Transactions on Pattern Analysis and Machine Intelligence*, 40(6): 1452–1464.

Appendix

Counterfactual Explanation via Nearest Unlike Neighbours

The Nearest-Neighbour Counterfactual Explainer (NNCE) method for generating counterfactual explanations is to identify the *nearest unlike neighbour* of a given instance x : the closest point x_{nn} in the training set that receives a different prediction under the target classifier (Guidotti 2024). The counterfactual explanation is x_{nnce} , the instance with the smallest such distance that leads to a different prediction.

To improve upon this baseline, the NICE algorithm (Nearest Instance Counterfactual Explanations) extends this approach by iteratively constructing counterfactuals through

feature substitutions from x_{nnce} . Starting from x , NICE explores combinations of feature changes using a depth-first search, replacing values with those from x_{nnce} to generate valid counterfactuals. Several variants of NICE allow for user-defined preferences: minimising the number of changed features (sparsity), minimising the total distance (proximity), or maximising data manifold plausibility. Unlike gradient-based methods, NICE is model-agnostic, applicable to any classifier, and guarantees explanation coverage.

Experimental Setup

Datasets. We present two experiments for the CIFAR benchmarks, one on CIFAR-10 and another on CIFAR-100 (Krizhevsky and Hinton 2009). Both of these experiments use the following four OOD datasets, following the methodology from fDBD: SVHN (Netzer et al. 2011), iSUN (Xu et al. 2015), Places365 (Zhou et al. 2018), and Textures (Cimpoi et al. 2014).

In section , we present experiments for ImageNet-200 (Zhang et al. 2024), which is a 200 class subset of the ImageNet-1K dataset (Deng et al. 2009). We use the following four OOD datasets: SSB-hard (Vaze et al. 2022), iNaturalist (Van Horn et al. 2018), Textures (Cimpoi et al. 2014), and OpenImage-O (Wang et al. 2022).

In section , we present a case study on generating explanations on the MNIST dataset (LeCun, Cortes, and Burges 1998). In order to create OOD points, we split the MNIST data by taking the first six classes (0-5) as ID inputs and the rest (6-9) as OOD.

Architectures. The experiments on the CIFAR datasets and ImageNet-200 are run on pre-trained ResNet-18 (He et al. 2016) models. We average our results over three separate training runs provided by OpenOOD (Yang et al. 2022). For MNIST, we train a three layer convolutional neural network (CNN) on the first six classes as described above. The CNN achieves 98% accuracy on the ID test set.

Baseline Methods. We compare our method against eight baseline methods. The first three methods compute OOD scores directly on the output of the DNN. MSP (Hendrycks and Gimpel 2017) calculates the maximum softmax probability of all inputs as an OOD score, ODIN (Liang, Li, and Srikant 2018) extends MSP through temperature scaling and adversarial perturbations, and Energy (Liu et al. 2020) calculates an energy score on the outputs of the DNN. A few methods utilise distance metrics, such as MDS (Lee et al. 2018), which estimates a Gaussian distribution over the latent space and uses the Mahalanobis distance for their score, KNN (Sun et al. 2022), which computes the distance to the k th nearest neighbour and fDBD (Liu and Qin 2024) which calculates the average distance to decision boundaries. We also include two other methods utilising different approaches: ViM (Wang et al. 2022) which calculates an OOD score based on the feature space and the logit space and DICE (Sun and Li 2022) which takes advantage of sparsification to only consider important weights to obtain an energy-based OOD score.

k	FPR95↓	AUROC↑	Avg Time (ms)
25	14.93	96.85	2.24
50	14.06	97.01	4.53
75	14.10	96.95	6.65
100	13.79	97.05	8.74

Table 4: Ablation study on CIFAR-100 OOD benchmarks using our method with NNCE averaged over OOD datasets SVHN, iSUN, Textures, and Places365 and averaged over three training runs, using the same ResNet-18 network as in Table 2. Here, k is the number of classes we compute counterfactuals for and thus, how many decision boundaries we consider in our distance metric. Avg Time (ms) refers to the milliseconds it takes to compute our OOD score on a machine equipped with a 28-core CPU with 512GB RAM. We average the computation time over 100 inputs.

Runtime Analysis on CIFAR-100

Our experiments on CIFAR-100 show favourable results, outperforming all baselines. We perform a runtime analysis of our method using NNCE on CIFAR-100 to further show the practical applicability of our approach. We consider a variation of our method whereby instead of computing counterfactual distances for all possible target classes, we compute only k counterfactuals. We choose the top k classes (excluding the predicted class) based on the output probability distribution from the DNN and compute the counterfactual distance to each of these classes. The choice of which counterfactuals to compute can instead be determined by the user, for example if some classes are deemed more important based on some domain knowledge.

In Table 4, we show results with our NNCE method on CIFAR-100 when computing counterfactuals for the top k classes for $k = 25, 50, 75$, and 100, the latter of which is equivalent to what we did in the previous section. We also include the average number of milliseconds our scoring method takes, averaged over 100 inputs when run on a 28-core CPU with 512 RAM.

In Table 4, we see that the FPR95 and the AUROC generally worsen as we reduce k , but interestingly $k = 50$ slightly outperforms $k = 75$. This suggests that the 25 extra classes we consider for $k = 75$ do not provide us with more information, and they may add a bit of noise to our scoring method.

Even with only 25 classes, our average result beats all the baselines from Table 2. In this case, an end user could determine the right trade-off between accuracy and runtime costs in determining the k that is best for a particular use case. We also hypothesize that this choice is highly dependent on the datasets used, and with some domain knowledge a user can select which k classes to use in the distance measure. For example, on CIFAR-100, we may decide that reducing k to 50 is worth the 0.27% worsening of the FPR95 if we also get a 4.21 millisecond runtime benefit. This ablation study provides insight into utilising this scoring method on larger datasets with more complex classes.

Comparing our runtime to other methods, fBDB shows

that their method can produce scores of 0.53 ms on CIFAR-10. Their experiments were run on a machine equipped with a Tesla T4 GPU. We do not expect our method to be faster than theirs. However, exploring more lightweight methods of implementing the counterfactual search and utilising GPUs would mitigate some of this runtime difference. To our knowledge, no counterfactual search methods are optimised for GPU hardware.

Counterfactual Explanation Case Study

In the evaluation section, we gave an example of our explanation framework on a novel input (an input whose ground truth class is unknown to the DNN). Below, we present an example of an OOD point that is a member of a known class but is unlike what the DNN has seen before.

In this case, we have a 5, which our CNN predicted to be a 0. Similarly to what we saw in the evaluation section, we put the input at the top, in this case, a 5, followed by the nearest like neighbours and the nearest unlike neighbours. We also have the distances between each neighbour and the original input below the images. It is interesting to note that the 5s class is closest to our input, even though this is not the predicted class. This insight can help us determine that this input should actually be classified as a 5. By comparing both like and unlike neighbours, we can conclude that this input is OOD, unlike what we have seen before. However, we can also see that the input is a member of one of the other known classes.

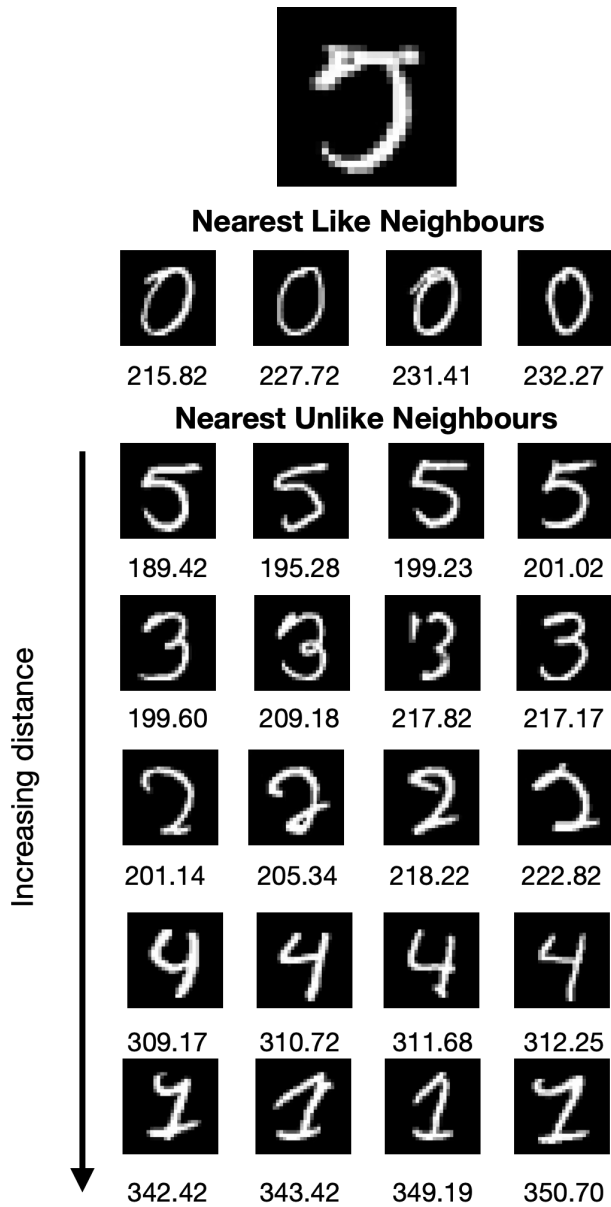


Figure 3: An example of an explanation our method can output. At the top, we have an OOD point, which is a 5 and a class our model is trained on. The model predicts this to be a 0. Below the 5, we present the four nearest like neighbours, which are the closest 0s in the training set to our OOD input. The leftmost 0 is the closest to this point, and the distance increases as we go to the right. Below this, we present each class’s four nearest unlike neighbours. The classes are ordered by how close they are to the original input, so the 5s are closest, followed by the 3s, and so on, with 1s being the furthest class. Within each class row, the leftmost image is the closest to the input, and the rightmost is the furthest. It is interesting to note that the input is closest to the 5s class than its predicted class. We present the distance between the nearest neighbour and the original input below each image. By utilising nearest like and unlike neighbours, we can reduce model over reliance and better understand why our detector identified this input as OOD.